Electrochimica Acta 462 (2023) 142752

Contents lists available at ScienceDirect

Electrochimica Acta

journal homepage: www.journals.elsevier.com/electrochimica-acta

Simultaneous local sensing of two chemical properties with dual soft probe scanning electrochemical microscopy

Gregorio Bonazza [a], Hubert H. Girault [b], Andreas Lesch [c,*], Salvatore Daniele [*,a]

[a] Department of Molecular Sciences and Nanosystems, Ca'Foscari University of Venice, 30123 Venice, Italy
[b] Laboratory of Physical and Analytical Electrochemistry (LEPA), École Polytechnique Fédérale de Lausanne (EPFL) Valais Wallis, Rue del'Industrie 17, 1950 Sion, Switzerland
[c] Department of Industrial Chemistry "Toso Montanari", University of Bologna, Viale del Risorgimento 4, 40136 Bologna, Italy

ARTICLE INFO

Keywords:
Soft microelectrodes
Dual microelectrodes
Scanning electrochemical microscopy
Potentiometric probe
Amperometric probe
pH microsensor
RNS microsensor

ABSTRACT

A new method for the rapid and economic fabrication of dual soft microelectrodes for Soft-Probe-Scanning electrochemical microscopy (Soft-Probe-SECM) and their use for the simultaneous local detection of locally generated species is presented. The process is based on encapsulating electrode wires, such as Pt, Au and carbon fiber, by UV-photo-polymerization of a dielectric material leading to two microdisc electrodes, which are individually addressable. Probe stability is realized by using a flexible plastic support. The thickness of the dielectric material that controls the distance between the microelectrodes and the substrate surface during lateral scans over a substrate in contact mode is highly controllable by the probe fabrication parameters. The thickness of the dielectric material of the soft probes fabricated here varies between 27 μm and 35 μm, while the two microelectrodes inter-distance varies between 180 μm and 250 μm. The dual soft probes combine Pt, Au and C microdiscs of different radii (12.5 μm for Pt and Au and 4 μm for C). The flexible selection of the electrode materials enables the fabrication of dual soft probes with electrode materials suitable to detect electro-active analytes of interest at solid/solution interfaces. The dual soft probes can be used in double amperometric, double potentiometric or mixed potentiometric-amperometric modes. As a proof-of concept of the latter mode, a dual platinum black/Pt (PtB/Pt)–iridium oxide/Au (IrO_x/Au) soft probe is used to image in real time the chemically induced dissolution of inkjet printed silver patterns in 0.2 mM HNO_3, generating locally reactive nitrogen species (RNS) and simultaneously changing the pH. RNS amounts are measured at 0.8 V (vs. Ag/AgCl, KCl, reference electrode) at the PtB/Pt microelectrode, while the corresponding pH changes are obtained from open circuit potential measurements with the IrO_x/Au microelectrode.

1. Introduction

The most common probes used in scanning electrochemical microscopy (SECM) are amperometric microelectrodes that are typically produced by sealing a metal wire of micrometer or sub-micrometer diameters in glass capillaries and, subsequently, exposing their cross-section ends, which include both the active metal surface and the surrounding insulator [1,2]. These kinds of probes, often also called SECM tips, allow monitoring the characteristics of a single species above a surface and, often, the corresponding signals are convoluted with the topographic characteristics of the surface under investigation. Complementary information on topography and local chemical characteristics of a sample surface, which is being addressed in the SECM community since ever, could be achieved by combining SECM with other scanning probe techniques, such as, for instance, atomic force microscopy (AFM) [3,4] and scanning ion conductance microscopy (SICM) [5–7]. Simultaneous information and imaging substrate properties can be gathered using multiple SECM probes, in which one electrode is used for the determination of tip-to-substrate distances (related to the surface topography) and the others for monitoring chemical properties [8,9]. Approaches to establish tip-to-substrate-distance control include vertical tip-position modulation methods, in which the probe can be vertically vibrated. The vibration is damped in close proximity to the sample surface, thus allowing to control the probe-substrate distance [10]. Non-electrochemical distance information can also be obtained by shear-force measurements [11]. The local reactivity of the substrate can

* Corresponding authors.
E-mail addresses: andreas.lesch@unibo.it (A. Lesch), sig@unive.it (S. Daniele).

https://doi.org/10.1016/j.electacta.2023.142752
Received 31 January 2023; Received in revised form 12 June 2023; Accepted 17 June 2023
Available online 18 June 2023

be resolved from the topography without hybridization of SECM with other techniques by using soft microelectrodes [9,12-19]. These probes are flexible and operated in a peculiar contact mode, in which they slide on the target substrate keeping a nearly constant working distance. This allows deconvoluting the topographic contribution from the desired reactivity signal. The increasing implementation of soft probes by various groups demonstrates the increasing popularity of Soft-Probe-SECM. Current soft probes show key advantages when micrometric resolution for substrate reactivity imaging is required and topographic substrate features are in the range of tens of micrometers. The current generation of soft probes cannot resolve nanometric features, which is the target of several electrochemical imaging techniques currently in the focus for nanocatalysis or single cell analysis [20–22]. Starting from the works of Girault, Wittstock and co-workers, several approaches for soft probe fabrication have been realized. The first and still most established version of soft probes is made of conductive carbon paste that is inserted into microchannels, which were fabricated by laser ablation into thin plastic foils [12]. After curing of the carbon paste, the solid carbon trace is covered and sealed using a thin polymer film, such as Parylene C [23]. Despite their wide range of applications, carbon paste-based soft probes can be disadvantageous, for instance when certain analytes, such as hydrogen peroxide, shall be detected, which suffers from slow electrode kinetics at carbon. One option is to deposit electrocatalysts on the soft carbon microelectrode [24]. As alternative soft probes, a freestanding platinum wire was insulated with Parylene C and used as soft SECM probe [25]. However, such probe deforms easily when being polished or mechanically cut as required to obtain a clean electrode surface, and has demonstrated less stable contact mode scanning due to its high flexibility. In another approach, a wide Pt foil was fixed with epoxy on a plastic sheet and then insulated from the other side with adhesive tape [13]. Using band microelectrodes as SECM probes requires however at least two perpendicular scanning directions and mathematical procedures to convert the signals into SECM images. Nanometer-thin gold microelectrodes were prepared by Aerosol Jet printing [26] or gold wire sealing between two adhesive tapes [17]. Soft probes are extremely suited for investigating large and irregular samples (e.g., curved, or soft surfaces). Linear arrays of soft microelectrodes have been fabricated to increase the areas that can be investigated reducing the experimental times sufficiently, which could be interesting for industrial applications as well as for biological samples. Indeed, soft probes have been employed to investigate biological samples, such as tissues and cells, as diagnostic tools for a variety of illnesses [14,15,17,27,28]. The complexity of the structure and morphology of biological samples typically complicates SECM procedures (e.g., to guarantee the essential constant tip-to-sample-distance) and the interpretation of the data and soft probes represent one possibility to study such systems in a straightforward manner [9,15].

In cancer prevention and control, an important role is played, among other parameters, by pH and the concentration of reactive nitrogen species (RNS) (i.e., NO, NO_2^-, ONO_2^-). Owing to intensive respiratory, CO_2 and acidic metabolites production from glycolysis and citric acid cycle, cancer cells are exposed to larger proton fluxes compared to normal cells. This causes a significant pH decrease in the extracellular medium [29–31]. The determination of pH levels is useful for exploring the general characteristics of a cancer, in order to improve diagnostics. Moreover, intracellular exchange of H^+ ions determines the ionization state of proteins and, consequently, their activity through key processes for cancer proliferation and metastasis. Therefore, the therapeutic potential of disturbing these sequences by targeting H^+-equivalent transporters is enormous, since the decrease of proton export from membrane induces apoptosis in cancer cells [30]. On the other hand, anomalous concentration of nitric oxide (NO) and of NO-related species has been detected in various types of cancer [32–38]. Data from many clinical and experimental studies have demonstrated that the role of NO in the carcinogenic process depends on its concentration. Nitric oxide is released from vascular endothelial cells. Therefore, cancer research and oncological practice would benefit from in-tumor (*in situ*) monitoring of NO concentration. From the above considerations, it appears that the development of a sensor system for the simultaneous detection of pH and NO active specie on tissues would be of great interest. Dual probes for SECM measurements have been proposed in the classical solid, thus non-flexible design within glass bodies, such as fluorinated epoxy diacrylate/Pt-IrO_x/Pt [39], Pt-solid state calcium ion-selective electrode [40] and Pt-IrO_x/Pt [41] for simultaneous amperometric and potentiometric uses. Single micro- and nanoelectrodes as SECM probes for sensing nitrogen species have been reported [42–44], but to the best of our knowledge not yet for flexible SECM probes.

This paper reports on the development of a dual soft probe, able to detect, at substrate/solution interfaces, both pH and RNS simultaneously with high spatial resolution. The economic and rapid fabrication of the dual soft SECM probes containing different electrode materials, such as platinum, gold and carbon, and electrode surface modifications by e.g. platinum black (PtB) and iridium oxides (IrO_x) is presented. The application of dual amperometric-potentiometric soft probes will be demonstrated for the detection of local variations of RNS at a PtB/Pt microelectrode and pH at a IrO_x/Au microelectrode. As a proof-of-concept, the dissolution of inkjet-printed silver patterns in dilute nitric acid, causing a local pH change and the formation of RNS, is followed by SECM imaging using the dual potentiometric-amperometric soft probe.

2. Experimental section

2.1. Materials

All the reagents were of analytical grade and, if not differently stated, they were used as received. Potassium nitrate (KNO_3), phosphate buffered saline (PBS, tablets), potassium carbonate (K_2CO_3), ferrocenemethanol (FcMeOH), hexachloroplatinic acid (H_2PtCl_6), potassium hexachloroiridate ($K_3[IrCl_6]$), oxalic acid ($C_2H_2O_4$), hydrogen peroxide (H_2O_2) and nitric acid (HNO_3) were from Sigma Aldrich. Polyethylene terephthalate (PET) foils were obtained from Folex. UV curable dielectric ink EMD 6200 was obtained from Sun Chemical and silver nanoparticle ink Silverjet DGP-40LT-15C (w/w 30–35%) from Sigma Aldrich. Platinum wire (diameter 25 μm), gold wire (diameter 25 μm) and carbon fiber (diameter 8 μm) were from Goodfellow. Polyimide (PI, Kapton) scotch tape was from Hopelight. Nitrogen was from Siad (≥ 99.99% pure) and was employed to purge the solutions when required.

2.2. Modification of Pt and Au microelectrodes of the dual soft probes

A custom-built aluminum cage containing four UV lamps (30 W, Philips) was used for UV photo-polymerization of the UV curable dielectric ink. PtB/Pt soft probes were prepared by electrodeposition of platinum black onto the smooth platinum microdisc of the dual soft probe in a 50% H_2PtCl_6 aqueous solution, as reported elsewhere [45]. The electrodeposition of platinum was carried out in a two-electrode cell configuration under potentiostatic conditions at −0.6 V vs. a Pt wire pseudo-reference electrode using a CompactStat potentiostat from Ivium Technologies. The amount of deposited PtB was controlled from the current/potential profiles recorded during the plating step [45]. The electrodeposition of hydrated iridium oxide (IrO_x) was performed onto the smooth gold microelectrode (IrO_x/Au) of the dual soft probes, using a two-step procedure [46,47] described in detail in the Supporting Information SI-1. The deposition solution was prepared by dissolving 0.4 mmol of K_3IrCl_6 in 25 mL of water and 0.5 mL of a 30% (w/w) H_2O_2 solution were then added for producing Ir(IV) species. After stirring for 30 min, 5.5 mM of $C_2H_2O_4$ were added for the formation of the $[Ir(COO)_2(OH)_4]_2$ complex. The solution was then made basic to pH 10.5 using K_2CO_3. The solution color changed from pale yellow to blue after four days indicating the complex formation. The first electrodeposition step was then carried out by applying a potential of 0.8 V vs. Ag/AgCl (sat. KCl) for 600 s, forming potentially IrO_x. In the second

electrodeposition step, the IrO_x-coated gold microelectrode was cycled consecutively for at least five cycles over the potential window from 0 to 0.8 V at 100 mV/s either to increase the amount of IrO_x deposited or to form the mixed Ir(IV)/Ir(III) oxides system.

2.3. Characterization methods of the dual soft SECM probes

Microscopic characterization was done by using a Keyence VK 8700 Laser Scanning Microscope (LSM) or by taking photographs. Unless otherwise stated, all electrochemical characterizations of electrodes and SECM measurements were performed in a three electrode cell arrangement using a customized scanning electrochemical microscope running under SECMx software (University of Oldenburg, Germany), comprising a CompactStat with peripheral port expander (Ivium Technologies), a Märzhäuser three-axes positioning system and an electronic sample tilt table (Zaber Technologies). Soft SECM probes were used as working electrodes, a Ag/AgCl (1 M KCl) electrode as reference electrode (RE) and a Pt wire as counter electrode (CE). All potentials herein are referred to the RE. For SECM measurements, the soft probes were mounted with a pre-defined angle with respect to the sample surface normal using a custom-built soft probe holder [48]. The probe angle i) avoided direct contact between the active parts of the soft microelectrode (i.e., the Au, Pt or carbon surface) and the surface of the substrate underneath, and ii) enabled stable "brushing" of the probe over the substrate surface during SECM probe scans over the substrate surface in contact mode. The analysis of SECM approach curves (vertical probe movements towards and away from the substrate) or horizontal scans for SECM line scans and SECM 2D imaging were carried out using MIRA software (University of Oldenburg, Germany).

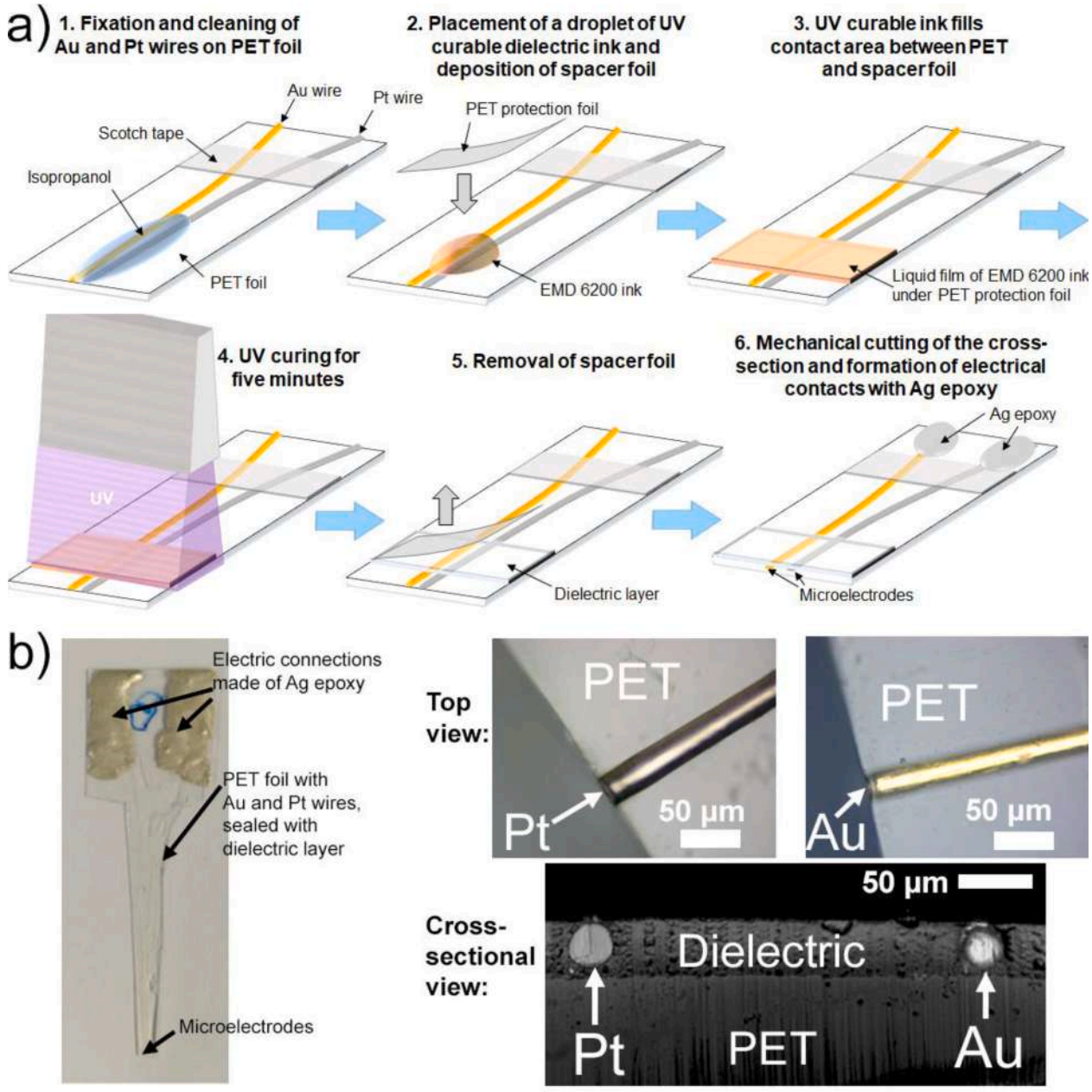

Fig. 1. Manufacturing procedure of dual soft probes for SECM as developed in this work. a) Schematic representation of individual fabrication steps as indicated by numbers 1 to 6. b) Optical micrographs of an as-fabricated dual Pt-Au soft probe for SECM. The radii, *a*, of the Pt and Au wires were 12.5 µm.

2.4. Inkjet printing of Ag patterns

Test samples were prepared by inkjet printing of Ag patterns on PET foil according to our previously developed protocols. A Ceradrop X-Serie CeraPrinter (Ceradrop) was used with a Q-Class Sapphire QS-256 printhead (Fujifilm Dimatix) containing 256 individually addressable nozzles with 80 pL nominal droplet volume. The design of Ag patterns (dot array and parallel bands) was created using the software CeraSlice (Ceradrop). Printing parameters, such as the waveform for actuation of the piezoelectric actuator of the printhead, droplet ejection frequency, distance between printhead and substrate, substrate temperature, droplets per inch, were optimized for stable droplet ejection and high-resolution Ag patterning. The substrate temperature during printing was set to 60 °C facilitating ink solvent evaporation and limiting ink spreading on the substrate. Immediately after printing, the Ag ink was cured using a high intensity light pulse from a xenon flash lamp using a PulseForge 1300 photonic curing system (NovaCentrix). After photonic curing, the substrates were used for electrochemical measurements without any further treatments.

3. Results and discussion

3.1. Preparation of dual soft probes

Soft dual SECM probes were prepared using a facile multi-step process developed herein (Fig. 1a), which thus differs significantly from the conventional soft probe fabrication procedure that has been established over recent years by us. The newly created process is highly flexible in terms of material selection and probe geometries (e.g., thickness of the insulation layer that determines the effective working distance) as presented in detail in the following. A thin plastic foil, such as PET, of micrometric thickness (e.g., 180 μm) was used as soft probe support with a lateral dimension of 5 cm (length) × 1 cm (width). Two wires of the desired microelectrode materials, in this work two among Pt, Au and C, were placed with a desired lateral distance between each other of >100 μm on the PET foil. At one side, the two wires were fixed on the PET by using PI scotch tape (step 1). On the other side, the two wires were cleaned by rinsing with isopropanol and left to dry at room temperature for about 10 min. Thereafter, a precisely defined volume between 2 μL and 4 μL of UV curable dielectric ink EMD 6200 were dropped on the uncovered wire-PET assembly (step 2). Thereafter, a non-adhesive PET cover foil in the shape of a rectangle of ~1 cm^2 area was temporarily released over the wire-PET assembly with deposited dielectric ink. Letting the cover foil being adsorbed by the UV curable ink and by the resulting capillary actions, the UV ink spread in a controlled manner over the PET support surface covering a rectangular surface area of about 1 cm^2 (step 3). The UV curable ink was then cured for 5 min using the UV lamp becoming a transparent solid (step 4). Afterwards, the non-adhesive PET cover foil was removed (step 5) leaving the dielectric solid with embedded wires well-adhered on the PET support. The dielectric layers were homogeneous and smooth with an even thickness ranging between 27 μm and 35 μm, depending on the volume of UV curable ink that was initially placed on the PET foil (i.e., 2 μL – 4 μL) and the size of the PET cover foil spreading the ink over the support. Obviously, the dielectric material should fully cover the electrode wires for the complete insulation of their lateral parts. Electric connection pads, for realizing the electrical connections with clamps necessary to make electrochemical measurements, were created beyond the PI scotch tape by depositing conventional silver epoxy, which was cured in an oven at 80 °C for about 3 h. The cross-section of the tip of the probe was created with a razor blade cut (step 6) in order to release two disk-shaped active microelectrodes for electrochemical measurements. Microscopic images of an as-fabricated Pt-Au dual soft probe are shown in Fig. 1b, displaying in particular the top views on the embedded Pt and Au wires as well as the side view on the cross-section. The entire probe can be cut into a V-shape to reduce the lateral extension of the tip and facilitate complete contact of the probe with the substrate during contact mode scanning. The inter-electrode distance was typically varied between 180 μm and 250 μm, which avoided significant overlapping of the diffusion layers of the two microelectrodes [23]. This is important when both microelectrodes are used simultaneously in amperometric mode when the response of one microelectrode could be affected by the flux of electro-active species created at the adjacent microelectrode. Instead, no problem arises when the two microelectrodes are employed in mixed amperometric and potentiometric mode.

3.2. Dual soft probes with different microelectrode active materials

The dual soft probe fabrication process developed herein is in particular flexible in terms of the selection of the electrode material as demonstrated in the following examples of three soft dual SECM probes: a dual Pt-Au soft probe (Fig. 2a), a dual Pt-Pt soft probe (Fig. 2b) and a dual Pt-C soft probe (Fig. 2c). The top-view micrographs (recorded by looking through the transparent dielectric layer encapsulating the electrode wires) demonstrate that the electrode wires have generally been placed rather parallel to each other. The exact distances between the two micro-discs exposed by mechanical cutting of the probe cross-section will depend on the location of cutting along the encapsulated wires and can be accurately measured by inspection of the cross-section using optical microscopy. The cyclic voltammograms (CVs), using a standard electro-active species, such as FcMeOH, demonstrate reasonable shapes for the dual soft SECM probes that were entirely made of flexible materials and cut with a scalpel blade. Identical diameters for Pt and Au, i.e., 25 μm, result in nearly identical plateau currents for the diffusion-controlled oxidation of FcMeOH (average (3.92 ± 0.15) nA) for the Pt and Au microelectrodes while the currents for the C-based microelectrode are reasonably lower (average (1.15 ± 0.07) nA) due to the smaller disk diameter of 8 μm. A diagnostic analysis of the CVs confirms the electrochemical characteristics that are, in general, comparable to those found with glass encapsulation (SI-2). Currents larger than those predicted by theory for microdiscs embedded in an infinite insulating plane are due to the fact that parts of the microdiscs (i.e., those embedded in the dielectric material, opposite to the PET, Fig. 1b, cross-sectional view), are subject to diffusion from behind the plane of the electrodes [49,50] (SI-2). In addition, minor variations in the currents of theoretically identical electrodes as shown in Fig. 2b for two Pt microelectrodes might be caused by the probe cutting leading potentially to a small deformation from a perfect disk into a slightly elliptic shape or a partially recessed/extruded Pt disk. In our previous works, it has been demonstrated how the responses of individual microelectrodes (MEs) of linear arrays of MEs during SECM operations can be calibrated for SECM imaging, which relates to the current responses as well as the relative positions of the individual microelectrodes to each other [51, 52].

3.3. Control of the probe geometry to reduce the effective working distance during SECM imaging

During SECM operations, soft probes are tilted in respect to the surface normal of the substrate surface. This is mainly done for two reasons: i.) to stabilize the probe position during lateral SECM scans in contact mode (which is realized in a brushing like manner) and ii.) to avoid that the active part of the microelectrode could get in physical contact with the substrate, which could cause electrode and substrate contamination known as “fouling”. The latter situation would be achieved in the case that the probe is perpendiculary oriented (i.e., the probe body is parallel to the surface normal of the substrate) and vertically approached to the substrate surface. Fig. 3a shows too examples of a thin and thick dielectric layer in respect to each other. During SECM operations in contact mode, the dielectic layer contacts the substrate surface (Fig. 3b). The thickness of the insulation layer, $th_{\text{dielectric}}$ (the reference level is the surface of the PET support),

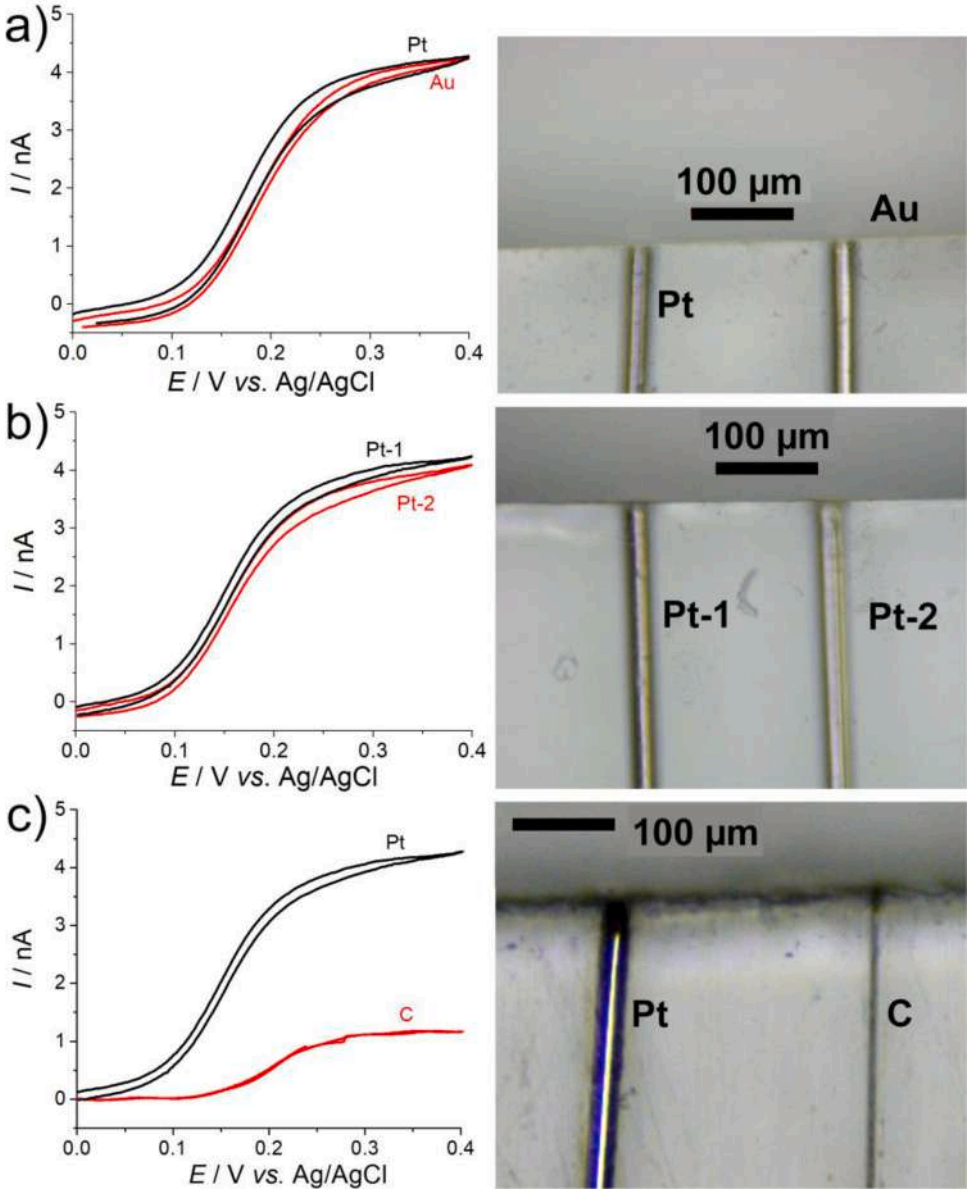

Fig. 2. Optical micrographs and CVs of Three Dual Soft SECM Probes with different electrode material combinations. a) Dual Pt-Au soft probe. b) Dual Pt-Pt soft probe. c) Dual Pt-C soft probe. Experimental conditions for CV: 1 mM FcMeOH in 0.1 M KNO_3, potential scan rate 20 mV/s.

represents therefore an important geometric characteristic of the soft probes as it affects the effective working distance d between the microdisc and the substrate surface. As thicker is the dielectric layer, the larger will be the working distance and the less will be the SECM signal resolution. The exact working distance will further depend on the probe angle α, which is determined by the tilt of the soft probe (SI-3). As it can be seen from the cross-sectional views in Fig. 3a, the electrode wires are completely surrounded by the dielectric material and do not contact the PET support so that the thickness of the insulation layer between microdisc and substrate, i.e., th_L, will be equal or inferior to ($th_{dielectric} - 2a$), where a is the radius of the microdisc electrode. Hence, th_L should be measured by using standard optical microscopy. Complete encapsulation of the metal wires by the dielectric material has shown the advantage of shielding completely the side walls of the electrode wires. The soft SECM probes were then electrochemically characterized by CV in an aqueous solution containing 1 mM FcMeOH (electroactive species) and 0.1 M KNO_3 (supporting electrolyte) (Fig. 3c, SI-2). As discussed above (and in more detail in SI-2), it is very well known, the thickness of the insulating sheath of a disk-shaped microelectrode affects the flux of the electro-active species by diffusion from the solution bulk to the active electrode surface [49,50]. Thick insulating sheaths block more efficiently the diffusion of the electro-active species from behind the probe. Therefore, the thinner is the insulating sheath, the larger will be the contribution of diffusion from behind the soft probe increasing the net diffusion of electro-active species and thus increasing also the recorded diffusion-controlled current at the microelectrode. In fact, as it can be seen in the CVs in Fig. 3c the plateau currents of the CVs for the oxidation of FcMeOH depends inversily on $th_{dielectric}$. With $th_{dielectric}$ = 35 µm, the plateau current is close to the theoretical value for an infinitely large insulating sheath, i.e., 3.76 nA, while the current for $th_{dielectric}$ = 27 µm was 9% larger (SI-2).

The soft probes with different thicknesses of the dielectric layer were then tested for standard Soft-Probe-SECM operations (Fig. 4). FcMeOH was used as redox mediator using the SECM feedback mode as an example of the most frequently used SECM modes. First, feedback mode approach curves were recorded, which are characterized by the vertical movement of the soft probe from the solution bulk down towards the substrate until the tip of the soft probe physically touches the substrate

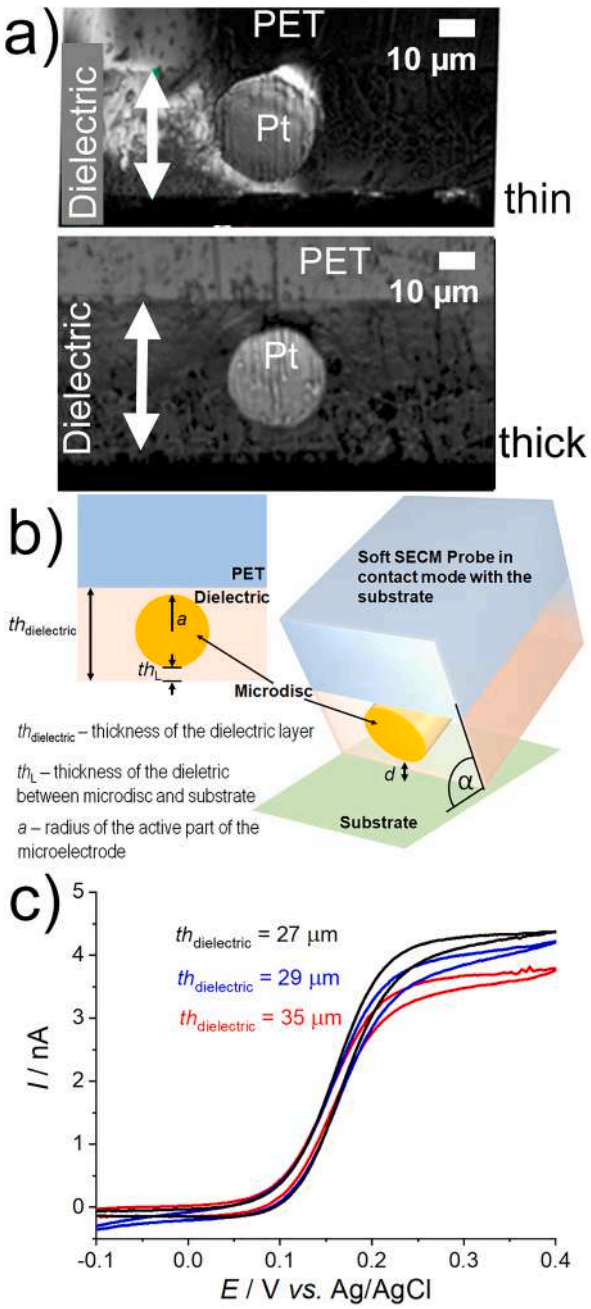

Fig. 3. a) Optical micrographs of an as-fabricated dual Pt-Au soft probe for SECM. The radii *a* of the metal wires were 12.5 µm. b) Schematic representation of the characteristic geometric soft probe parameters $th_{dielectric}$, th_L, *a*, *d* and *α*. c) Cyclic voltammogram recorded in the bulk solution using three different Pt soft probes with identical radius ($a = 12.5$ µm) but three different th_L values, i.e., 27 µm (black curve), 29 µm (blue curve) and 35 µm (red). Experimental conditions: potential scan rate 20 mV/s, measurement solution 1 mM FcMeOH in 0.1 M KNO_3.

surface and starts sliding "forward" over the substrate (probe translation details in SI-3). Second, SECM imaging in contact mode was carried out, which is the lateral scanning of the probe over the substrate surface in a brushing like manner (SI-3). Once a line scan has been completed, the soft probe is lifted into the solution not being any more in contact with the substrate and relocated onto the substrate surface at the desired coordinate for the subsequent line scan. Because the soft probe is in physical contact with the substrate, in theory, it could cause mechanical stress that could delaminate the thin polymer films of the soft probe. Therefore, SECM imaging with stable probe responses is also a proof of the mechanical stability of the soft probes as fabricated herein. Feedback mode approach curves, recorded over an insulator and conductor, with three soft probes with different $th_{dielectric}$ are shown in Figs. 4a,b, respectively. FcMeOH was oxidized to $FcMeOH^+$ at the soft probe and reduced back to FcMeOH at a large conductive surface when being positioned in close proximity to the soft probe. The recorded feedback currents, normalized by the steady-state diffusion-controlled plateau current for FcMeOH oxidation (here with an applied probe potential $E_P = 0.3$ V) when the soft probe is positioned in the solution bulk (I_{bulk}), are plotted as a function of the height of the probe h_P rather than the working distance *d*, as it has been established for soft SECM probes [23]. All soft probes have in common that after physical contact with the substrate and while being slid "forward" the effective working distance remains nearly constant. This is valid for h_P values equal or inferior to 0, where the recorded probe current in the approach curve creates a plateau (Fig. 4a,b). The feedback mode approach curves over the insulator show a decrease in current due to the physical blocking of the diffusion of FcMeOH by the inert substrate that gets closer to the soft probe. The contrary is observed over the surface of a conductor, at which FcMeOH gets regenerated by the reduction of $FcMeOH^+$ creating thus an additional flux of FcMeOH to the soft probe tip, which gets more efficient the closer the soft probe and the conductive substrate are positioned relative to each other. As it can be seen clearly for the approach curves, a thinner dielectric layer decreases the effective working distance at $h_P \leq 0$ and enhances the discrimination between currents caused by hindered diffusion and redox mediator regeneration. Therefore, thinner dielectric layers are preferred as they increase the SECM signal resolution (difference in current over conductor and insulator). As it is known from SECM approach curves over insulators and conductors using conventional solid disc-shaped microelectrodes, the change in current during an approach curve in close vicinity to the substrate is much more pronounced compared to the insulator due to the increasing effect of redox mediator recycling [53]. This can be seen in the approach curves of the soft probes herein (recorded current as a function of the probe distance h_P, not working distance *d*) where thinner dielectric layers changed the current over distance response close to the substrate surface more effectively over the conductor.

Thereafter, SECM imaging of Ag patterns was performed (Fig. 4c) to evaluate the general SECM scanning resolution and in particular the mechanical stability of the soft probes fabricated in the way described *vide supra* under repetitive contact mode operations. The probe translation rate that was selected in this work was relatively slow (i.e., 20 µm/s) in order to not disturb the diffusion layer by possible convection, even though it has been reported that scanning speeds with soft contact mode probes can generally be faster than for traditional SECM [16]. Slower probe translation rates didn't show any change in the response suggesting stable diffusion. For SECM imaging, the soft probe is brushed unidirectionally over the surface. A lift-off routine has been implemented into the software to retract the probe into the solution bulk during reverse scanning and positioning to the start coordinate of the subsequent line scan. This operation is carried out in order to avoid probe bending when inverting the scanning direction, a procedure that can create strong mechanical forces to the tip of the probe, as well as to the sample surface. As it can be seen, the dielectric layer was stable during all operations, excluding delamination and abrasion of the dielectric ink. The Ag bands were clearly resolved as result of redox mediator regeneration. SECM imaging of the Ag dot array revealed one particular characteristic. Each dot of the array was created by printing one single droplet of Ag ink. Inkjet printing of single droplets and subsequent thermal curing for solvent evaporation, material solidification and adhesion to the substrate leads often to the well-known coffee ring effect. Different evaporation rates of the solvent across the deposited ink droplet accumulates the major part of Ag nanoparticles at the rim of the droplet, depleting the center. This phenomenon is well-known in the literature and leads to the coffee ring effect [54]. The optical images in Fig 4c (left) clearly show this effect, in particular by the progressive

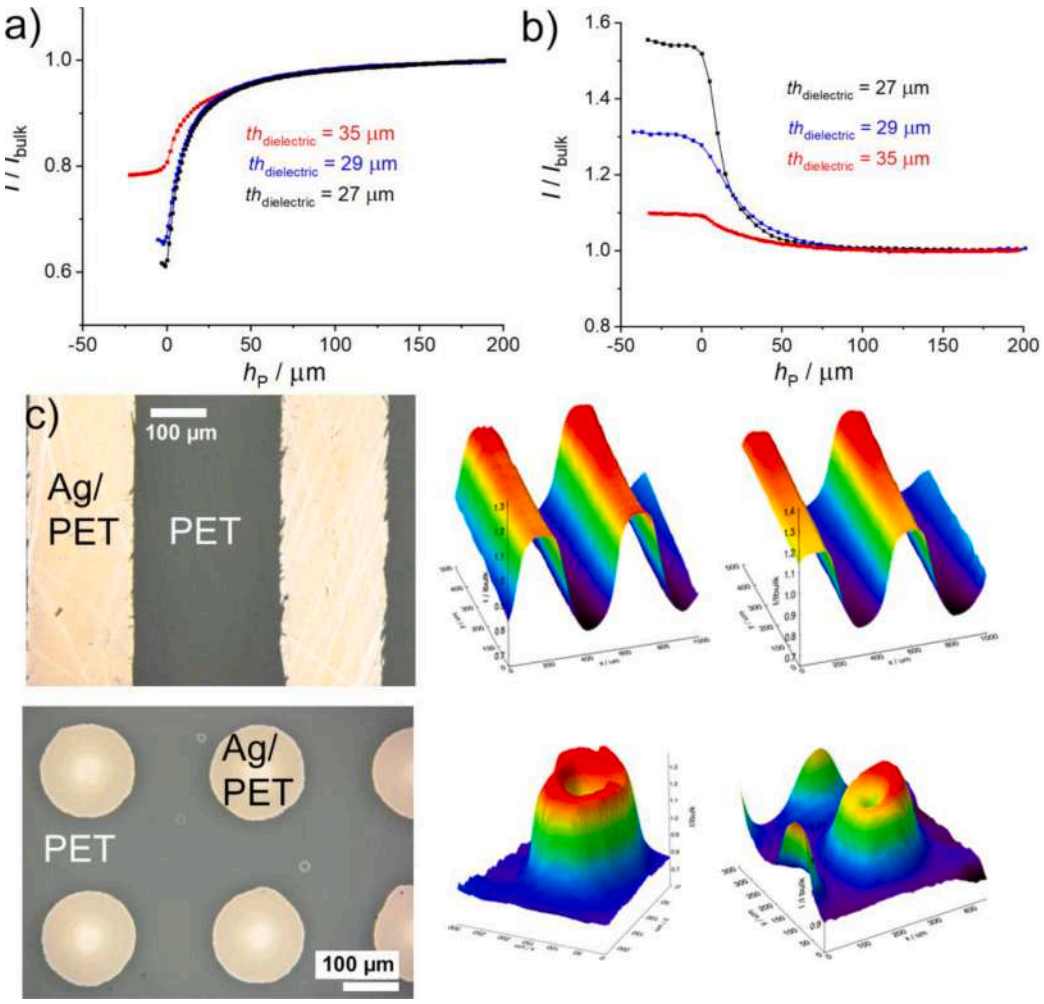

Fig. 4. Soft-Probe-SECM of the soft probes prepared herein using approach curves and imaging (probe currents were normalized by the probe bulk current). Approach curves over glass (a, insulator) and glassy carbon (b, conductor) using a Pt soft probe with different $th_{dielectric}$: 27 µm (black), 29 µm (blue) and 35 µm (red). c) Optical images (left) and feedback mode SECM images (rigth, interpolated data points) of inkjet printed Ag patterns on PET foil using a dual Au-Pt soft probe. Experimental conditions: 1 mM FcMeOH in 0.1 M KNO_3, E_P = 0.3 V, probe translation step sizes: 1 µm for approach curves and 10 µm for SECM images, lateral probe translation rates: 5 µm/s for SECM approach curves and 20 µm/s for SECM images.

color change from yellow to white. Consequently, the local conductivity and thus the ability to regenerate the redox mediator in the center of the Ag spot is lower than that at the rim. This can be clearly seen in the feedback mode SECM images (Fig. 4c, right) where the lower redox mediator regeneration rate is seen as a "hole" in the center of the Ag spots. Therefore, the dual soft probe clearly demonstrated its applicability for conventional Soft-Probe-SECM measurements. The SECM images were constructed from interpolated data. Line scan analyses with non-interpolated data, demonstrating response stability during scanning, will be shown in the following section. Both probes image areas that are separated by the lateral distance between the two microelectrodes, generally ~200 µm. As we have shown in previous works, knowing the distance between two probes enables merging of two images into a single image using data analysis software [51,52]. Alternatively, one probe can be used to create a first image and then the second probe after lateral displacement can be used to create subsequently a second image of the same area. Differences in the responses of the two microelectrodes caused for instance by variations of $th_{dielectric}$ would be calibrated as we have previously shown for linear arrays of eight microelectrodes [51,52].

Since in SECM imaging the dual soft probes are brushed various times over the substrate, modification of the dielectric layer (or contamination of the microdisc surfaces) can theoretically occur, but will depend on the substrate surface that is being investigated. If such effect would occur, repeated measurements made in the same area of the substrate as done during SECM imaging would produce much different responses, which were not observed. In this work, to ascertain the stability of the dual soft probes, especially the $th_{dielectric}$, and their further use, CVs were recorded in bulk solution containing the redox mediator before and after series of SECM imaging measurements to understand the condition of the electrodes. SECM responses shown in this work were not affected by problems due to $th_{dielectric}$ stability or other problems, such as chemical contamination of the active micoelectrode surfaces.

3.4. Dual soft probes for SECM imaging in simultaneous amperometric and potentiometric mode

As a proof-of-concept, a dual soft SECM probe was applied for imaging simultaneously local pH changes and the correlated local formation of RNS during the corrosion of Ag patterns in an acidic environment. The dual soft probes employed here integrated Pt and Au microelectrodes, whose surfaces were modified to impart the desired sensing abilities. In particular, the Pt microdisc was coated with a layer of PtB (PtB/Pt microelectrode, see experimental section) for the amperometric detection of RNS. The gold microdisc was coated with a layer of IrO_x (Au/IrO_x, see experimental section and SI-5) for the potentiometric monitoring of pH (SI-6). This configuration, combining amperometric and potentiometric detection methods, avoided mutual perturbation of the local chemical environment, as the potentiometric part acted as a passive probe [2]. The Pt and Au modified microdisc electrodes of the dual soft probe were characterized as illustrated in detail in SI-4, SI-5 and SI-6.

The Au microdisc was coated with hydrated IrO_x to exploit its sensitivity towards pH changes. In fact, the potential of the Ir(IV)/Ir(III) redox couple depends on the activity of protons and hence on the solution pH, according to the following redox process [46,55,56]:

$$2\left[IrO_2(OH)_{2-x}(2+x)H_2O\right]^{(2-x)-} + (3-2x)H^+ + 2e^- \rightleftharpoons \left[Ir_2O_3(OH)_{3-x}(3+x)H_2O\right]^{(3-x)-} + 2H_2O \quad (1)$$

The hydrated IrO_x–based pH sensor can display super-Nernstian pH response, i.e., the slope of the pH response as a function of pH enhances the theoretical value of −59 mV/pH reaching up to −90 mV/pH at room temperature [46]. Herein, the sensitivity of the soft IrO_x/Au microelectrode towards pH was −61 mV/pH, which was within the range of other reported IrO_x electrodes [57–59]. The response time of the sensor was within 1–1.5 s (Fig S6a, inset), short enough to ensure the achievement of the equilibrium potential while scanning the soft probe. In addition, the measured open circuit potential (E) displayed enough long-term stability (Fig. S6), which is an important aspect for SECM imaging.

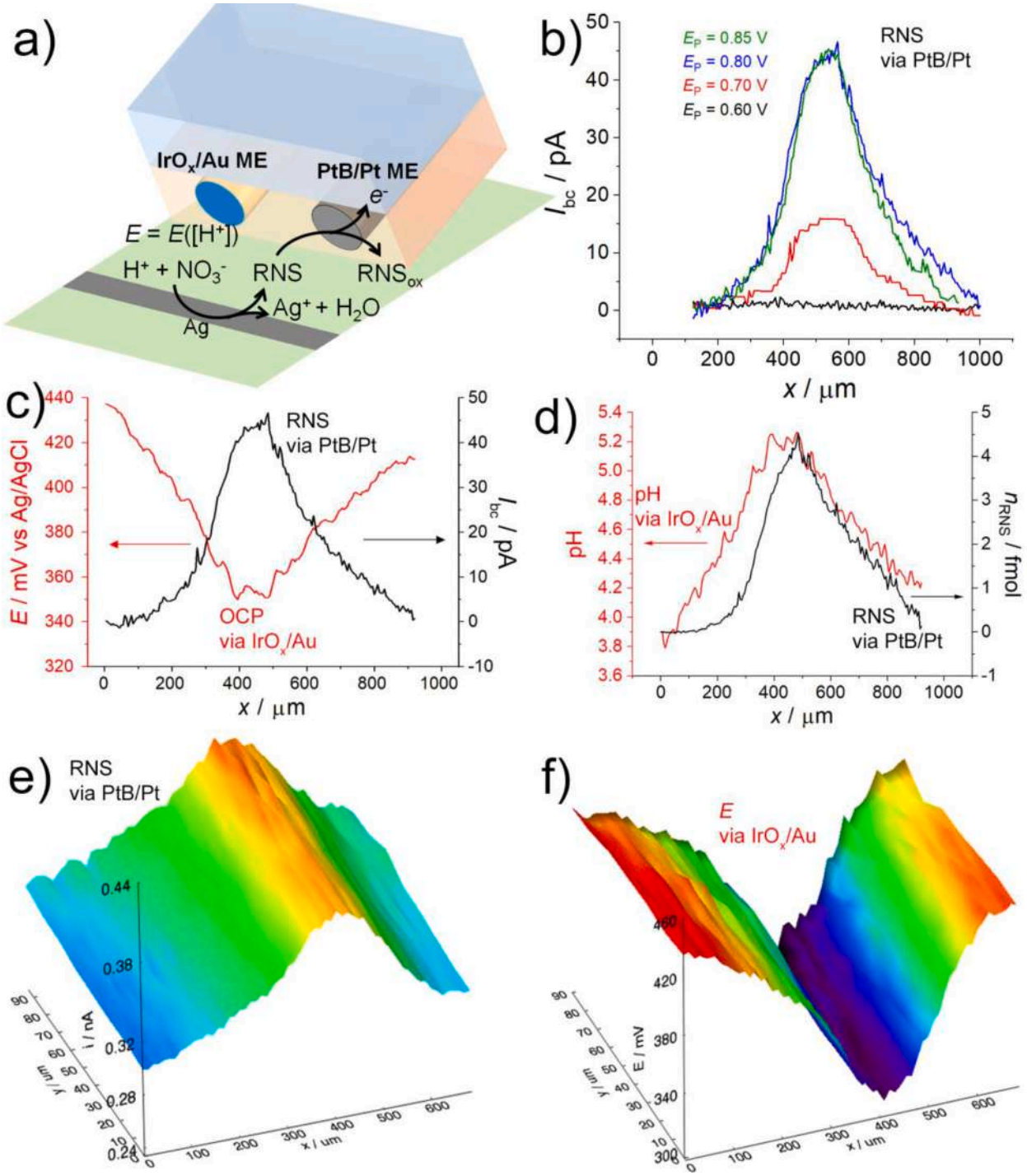

Fig. 5. Simultaneous real time mapping of silver corrosion using a soft dual amperometric-potentiometric SECM probe of PtB/Pt and IrO_x/Au, respectively. a) Schematic representation of the detection principle. b) RNS profiles as amperomeric line scans (baseline-corrected) by applying different potentials E_P at the PtB/Pt microelectrode. c) Simultaneous amperometric (E_P = 0.8 V) and potentiometric line scans over a corroding Ag line on PET (non interpolated data points). d) Data from (c) with I_{bc} converted into n_{RNS} and E converted into pH values according to the calibration shown in SI-6. e) Amperometric SECM image for RNS profiling (not baseline-corrected, interpolated data points), E_P = 0.8 V. f) Potentiometric SECM image for pH profiling. Probe translation speed 5 µm/s. Measurement solution 0.2 mM HNO_3 and 0.1 M KNO_3.

The simultaneous SECM monitoring of RNS and pH was established above an inkjet-printed Ag band of 150 μm width on PET, submerged in 0.2 mM HNO_3. Under these conditions, Ag corrosion sets in spontaneously according to Eq. (2) [60,61], dissolving Ag and forming nitric oxide ($^{\cdot}NO$):

$$3Ag + 4HNO_3 \rightarrow 3Ag^+ + 3NO_3^- + 2H_2O + {}^{\cdot}NO \quad (2)$$

In the presence of oxygen, other RNS can be formed, such as NO_2^-, according to the reaction pathways shown in Eqs. (3)–(7) [62].

$$^{\cdot}NO + O_2 \rightleftharpoons ONOO^{\cdot} \quad (3)$$

$$ONOO^{\cdot} + {}^{\cdot}NO \rightarrow ONOONO \quad (4)$$

$$ONOONO \rightarrow 2\,^{\cdot}NO_2 \quad (5)$$

$$^{\cdot}NO_2 + {}^{\cdot}NO \rightleftharpoons N_2O_3 \quad (6)$$

$$N_2O_3 + H_2O \rightarrow 2NO_2^- + 2H^+ \quad (7)$$

Reactions (4)–(6) are very fast resulting in species with very short lifetimes [62]. Therefore, the species, which are most likely being detected with the approach and resolution time of the method employed herein, are $^{\cdot}ONOO$, $^{\cdot}NO$, NO_2^-. These species can be oxidized at different potentials, varying from 0.45 to 0.85 V vs. Ag/AgCl (NaCl), and their stability depends on pH [42,43,63]. In particular, $^{\cdot}ONOO$, and $^{\cdot}NO$ are oxidized at potentials ≤ 0.6 V and NO_2^- is oxidized at potentials above 0.6 V, reaching a steady-state limiting current at about 0.8 V [42].

The overall spontaneous Ag corrosion involves a change of both pH and RNS amount, which can be monitored by SECM when scanning perpendicularly across a Ag microband (Fig. 5). The detection concept is schematically shown in Fig. 5a. However, it must be noted that the dual sensing is done by a local separation of about 100 μm to 180 μm, depending on the probe dimensions, due to the separate locations of the two microelectrodes (*vide supra*).

The optimal potential to reveal RNS under the experimental conditions employed herein was verified by recording amperometric line scans over a corroding silver band in dilute HNO_3 solution by applying at the PtB/Pt different potentials, i.e., between 0.4 V and 0.85 V. As evident from Fig. 5b, which shows background corrected currents I_{bc} (background currents were generally around 300 pA) up to 0.6 V, it is suggested that, under the employed conditions, $^{\cdot}ONOO$, $^{\cdot}NO$ contribute to the overall current to a negligible extent. Instead, by increasing the potentials above 0.6 V, the current signals increased over the center of the Ag, reaching a maximum current at 0.8 V (Fig. 5b). This suggests that the main specie responsible of the electrode process is NO_2^-. The above current against distance profile, recorded at 5 μm/s was essentially the same also at a higher translation speed (i.e., 10 μm/s, Fig. S7). From the current and the scan speed of the soft probe, the integral involved in the *I* vs. *x* profile (i.e., the charge *Q,* as *x* is also related to time, depending on the translation speed) could be evaluated, and from the Faraday law the number of moles of RNS could be obtained. A similar approach was employed to establish fluxes of RNS above a macrophage culture [64].

The open circuit potential at the IrO_x/Au soft probe changed during the line scan according to the local H^+ activity variation over the corroding Ag line as shown as an example in Fig. 5c (red line). In particular, pH increased from the border to the center of the Ag band, indicating a locally higher decrease of H^+, due to the overall reaction, Eq. (2), overwhelming the local H^+ production, due to reaction, Eq. (7).

Based on the above results, for the dual SECM operations, the platinized Pt microelectrode was kept at +0.80 V, where RNS oxidation provided the highest currents [43,63,65] (Fig 5c, black line), while the IrO_x/Au microelectrode was kept at open circuit and reflected the change of H^+ activity. The simultaneous monitoring of the amount of RNS and pH (i.e., after converting *E* values from Fig. 5C to pH, using the *E* vs. pH plot in Fig. S6b), was then tested in 0.2 mM nitric acid and Fig. 5d shows the estimated amounts of RNS (as n_{RNS} in fmol) and pH changes. As evident, n_{RNS} and pH vary, as expected, giving maximum values almost in the same location. Which means that where the RNS formation, through reactions (2)–(7), is the largest, pH is the highest. It can be noticed that the responses over lateral distance profiles of the two species do not overlap perfectly in Fig. 5d. This might have been caused by small geometric variations of the two chemically modified microelectrodes (i.e., exact working distance, geometries of the microelectrode modifying films of PtB and IrO_x, etc.). To exclude any artifacts in the above measurements, control experiments were performed with the dual modified soft probes above a pristine Ag band immersed in 0.1 M KNO_3, where corrosion of Ag should be negligible or would proceed to a much slower extent (SI-8). Background currents, with a slight drift towards higher values, were essentially recorded across the Ag band, whereas *E* decreased while passing from the insulating PET to the Ag band. The open circuit potential variation corresponded to an increase of 0.2 pH units. These findings are conceivably due to slow corrosion of the Ag due to oxygen and formation of small amounts of reactive oxygen species (ROS) that are, conceivably, responsible of the small current drift, as they also can be oxidized at the potential applied at the PtB/Pt [37,42]. The formation of ROS involves consumption of protons and pH rise, which can be monitored by the IrO_x/Au microelectrode. Instead, RNS, which could be generated from NO_3^- of the supporting electrolyte, are below the detection limit of the PtB/Pt-based RNS sensor.

Finally, full 2D images for the simultaneous RNS and *E* (i.e., pH) monitoring were recorded as displayed in Fig 5e and 5f, respectively, which further highlights the suitability for the two parameters monitoring using the dual soft probes proposed here.

4. Conclusion

To conclude, dual soft microelectrodes as probes for Soft-Probe-Scanning electrochemical microscopy (Soft-Probe-SECM) have been presented. The soft probes were fabricated herein following a novel procedure, which, at variance of the previous already available approaches, allows obtaining multiple, independently connected probes made of different materials. A key step of the fabrication is the encapsulation of electrode wires of micrometric diameters into a dielectric flexible polymer that is formed by UV-photopolymerization of a UV curable ink within just five minutes of light exposure. A high control of the thickness of the dielectric layer was reached by controlling the ink volume and using an ink-spreading plastic cover foil, which is temporarily placed on the assembly and transparent to wavelengths required for the photopolymerization. During SECM operations in contact-mode, such as line scans and surface reactivity imaging, the dual soft probes offered a remarkable mechanical and chemical stability, which was especially seen by the feedback mode images obtained over inkjet printed silver patterns. In order to create selective dual probes, the surfaces of the electrodes of a dual Au-Pt soft probe were electrochemically modified with a layer of iridium oxides and platinum black, respectively, to fabricate a potentiometric pH microsensor and an amperometric RNS microsensor within the same probe. As a proof-of-concept on the usefulness of the dual probes developed here, they were used to detect locally proton activity and fluxes of reactive nitrogen species over a corroding Ag pattern. These kinds of dual probes are foreseen for their application to investigate in particular large and irregular biological specimens, including cancer tissue and biofilms where local events with micrometric resolution are of interest. We foresee in particular applications for studying engineered and printed 3D cell models (i.e., live cell aggregates, tissues and organs) that get more and more into the focus of current research and being increasingly investigated by electrochemical methods [66]. Soft flexible microelectrodes are ideal to be scanned on the surfaces of such specimens as they are ideally suited to investigate delicate, gel-like surfaces.

Finally, we would like to comment on general advantages and limitations of the dual soft probes presented herein. The dual soft probes can be easily fabricated, using simple and low cost materials. The surface

of the microdiscs can be renewed simply by cutting the bottom of the tip using a sharp blade, in particular in case of possible electrode fouling, which is a general electrochemical phenomenon and therefore not limited to the soft dual SECM probes. On the other hand, because of the inter-electrode distance of a few hundred micrometers, the simultaneous detection of two electrochemical events in exactly the same location is hindered, as the second microelectrode has to be translated over the same coordinates with a delay. In addition, as for many other disposable, micro-fabricated electrode systems fabricated using inks, sensor stability in aggressive organic solvents can be limited and should be evaluated before use.

Author contributions

G.B. performed the SECM experiments and general soft probe characterizations. G.B. and A.L. prepared the soft SECM probes. G.B., H.G., A.L. and S.D. drafted the manuscript. A.L. and S.D. wrote the manuscript. G.B., H.G., A.L. and S.D. designed the research. A.L. and S.D. supervised the research. All authors have given approval to the final version of the manuscript.

Declaration of Competing Interest

The authors declare that they have no known competing financial interests or personal relationships that could have appeared to influence the work reported in this paper.

Data availability

Data will be made available on request.

Supplementary materials

Supplementary material associated with this article can be found, in the online version, at doi:10.1016/j.electacta.2023.142752.

References

[1] D. Polcari, P. Dauphin-Ducharme, J. Mauzeroll, Scanning Electrochemical Microscopy: a Comprehensive Review of Experimental Parameters from 1989 to 2015, Chem. Rev. 116 (2016) 13234–13278.

[2] A.J. Bard, M.V. Mirkin, Scanning Electrochemical Microscopy, 3rd ed., CRC Press, 2022.

[3] C. Kranz, G. Friedbacher, B. Mizaikofft, A. Lugstein, J. Smoliner, E. Bertagnolli, Integrating an ultramicroelectrode in an AFM cantilever: combined technology for enhanced information, Anal. Chem. 73 (2001) 2491–2500.

[4] S. Daboss, J. Lin, M. Godejohann, C. Kranz, Redox Switchable Polydopamine-Modified AFM-SECM Probes: a Probe for Electrochemical Force Spectroscopy, Anal. Chem. 92 (2020) 8404–8413.

[5] B. Chen, D. Perry, A. Page, M. Kang, P.R. Unwin, Scanning Ion Conductance Microscopy: quantitative Nanopipette Delivery-Substrate Electrode Collection Measurements and Mapping, Anal. Chem. 91 (2019) 2516–2524.

[6] K. Cremin, B.A. Jones, J. Teahan, G.N. Meloni, D. Perry, C. Zerfass, M. Asally, O. S. Soyer, P.R. Unwin, Scanning Ion Conductance Microscopy Reveals Differences in the Ionic Environments of Gram-Positive and Negative Bacteria, Anal. Chem. 92 (2020) 16024–16032.

[7] X. Xu, D. Valavanis, P. Ciocci, S. Confederat, F. Marcuccio, J.F. Lemineur, P. Actis, F. Kanoufi, P.R. Unwin, The New Era of High-Throughput Nanoelectrochemistry, Anal. Chem. 95 (2023) 319–356.

[8] C. Wei, A.J. Bard, G. Nagy, K. Toth, Scanning Electrochemical Microscopy. 28. Ion-Selective Neutral Carrier-Based Microelectrode Potentiometry, Anal. Chem. 67 (1995) 1346–1356.

[9] T.E. Lin, S. Rapino, H.H. Girault, A. Lesch, Electrochemical imaging of cells and tissues, Chem. Sci. 9 (2018) 4546–4554.

[10] M.A. Edwards, A.L. Whitworth, P.R. Unwin, Quantitative analysis and application of tip position modulation-scanning electrochemical microscopy, Anal. Chem. 83 (2011) 1977–1984.

[11] Y. Lee, A.J. Bard, Fabrication and characterization of probes for combined scanning electrochemical/optical microscopy experiments, Anal. Chem. 74 (2002) 3626–3633.

[12] F. Cortés-Salazar, M. Träuble, F. Li, J.M. Busnel, A.L. Gassner, M. Hojeij, G. Wittstock, H.H. Girault, Soft stylus probes for scanning electrochemical microscopy, Anal. Chem. 81 (2009) 6889–6896.

[13] G.D. O'Neil, H.W. Kuo, D.N. Lomax, J. Wright, D.V. Esposito, Scanning Line Probe Microscopy: beyond the Point Probe, Anal. Chem. 90 (2018) 11531–11537.

[14] S. Darvishi, H. Pick, T.E. Lin, Y. Zhu, X. Li, P.C. Ho, H.H. Girault, A. Lesch, Tape-Stripping Electrochemical Detection of Melanoma, Anal. Chem. 91 (2019) 12900–12908.

[15] S. Darvishi, H. Pick, E. Oveisi, H.H. Girault, A. Lesch, Soft-probe-scanning electrochemical microscopy reveals electrochemical surface reactivity of E. coli biofilms, Sens. Actuat. B Chem. 334 (2021).

[16] A.E. Dorfi, J. Yan, J. Wright, D.V. Esposito, Compressed Sensing Image Reconstruction of Scanning Electrochemical Microscopy Measurements Carried out at Ultrahigh Scan Speeds Using Continuous Line Probes, Anal. Chem. 93 (2021) 12574–12581.

[17] Y.H. Lin, C.N. Tsai, P.F. Chen, Y.T. Lin, S. Darvishi, H.H. Girault, T.Y. Lin, M. Y. Liao, T.E. Lin, AI-Assisted Fusion of Scanning Electrochemical Microscopy Images Using Novel Soft Probe, ACS Measure. Sci. Au 2 (2022) 576–583.

[18] H. Chen, X. Kong, D. Wang, M. Zhang, Flexible Disk Ultramicroelectrode for High-Resolution and Substrate-Tolerable Scanning Electrochemical Microscopy Imaging, Anal. Chem. 94 (2022) 17320–17327.

[19] T.E. Lin, Y. Zhu, Y.T. Hsu, F.Y. Liu, Y.P. Lin, C.M. Cheng, In situ detection of multitarget impurities on contact lens by electrochemical scanning probe, Sens. Actuat. B Chem. 374 (2023).

[20] T. Kai, C.G. Zoski, A.J. Bard, Scanning electrochemical microscopy at the nanometer level, Chem. Commun. 54 (2018) 1934–1947.

[21] X. Wang, G. Askarova, M.V. Mirkin, Electrochemical microscopy at the nanoscale, Front. Nanosci. (2021) 129–202.

[22] J.F. Lemineur, H. Wang, W. Wang, F. Kanoufi, Emerging Optical Microscopy Techniques for Electrochemistry, Annu. Rev. Anal. Chem. (2022) 57–82.

[23] F. Cortés-Salazar, D. Momotenko, A. Lesch, G. Wittstock, H.H. Girault, Soft microelectrode linear array for scanning electrochemical microscopy, Anal. Chem. 82 (2010) 10037–10044.

[24] M.M. Pribil, F. Cortés-Salazar, E.A. Andreyev, A. Lesch, E.E. Karyakina, O. G. Voronin, H.H. Girault, A.A. Karyakin, Rapid optimization of a lactate biosensor design using soft probes scanning electrochemical microscopy, J. Electroanal. Chem. 731 (2014) 112–118.

[25] F. Cortés-Salazar, H. Deng, P. Peljo, C.M. Pereira, K. Kontturi, H.H. Girault, Parylene C coated microelectrodes for scanning electrochemical microscopy, Electrochim. Acta 110 (2013) 22–29.

[26] A. Lesch, D. Momotenko, F. Cortés-Salazar, I. Wirth, U.M. Tefashe, F. Meiners, B. Vaske, H.H. Girault, G. Wittstock, Fabrication of soft gold microelectrode arrays as probes for scanning electrochemical microscopy, J. Electroanal. Chem. 666 (2012) 52–61.

[27] T.E. Lin, A. Bondarenko, A. Lesch, H. Pick, F. Cortés-Salazar, H.H. Girault, Monitoring Tyrosinase Expression in Non-metastatic and Metastatic Melanoma Tissues by Scanning Electrochemical Microscopy, Angew. Chem. Int. Ed. 55 (2016) 3813–3816.

[28] T.E. Lin, Y.J. Lu, C.L. Sun, H. Pick, J.P. Chen, A. Lesch, H.H. Girault, Soft Electrochemical Probes for Mapping the Distribution of Biomarkers and Injected Nanomaterials in Animal and Human Tissues, Angew. Chem. Int. Ed. 56 (2017) 16498–16502.

[29] A. Hulikova, R.D. Vaughan-Jones, P. Swietach, Dual role of CO2/HCO3- buffer in the regulation of intracellular pH of three-dimensional tumor growths, J. Biol. Chem. 286 (2011) 13815–13826.

[30] M. Damaghi, J.W. Wojtkowiak, R.J. Gillies, pH sensing and regulation in cancer, Front. Physiol. 4 (2013), 370.

[31] F. Manig, K. Kuhne, C. von Neubeck, U. Schwarzenbolz, Z. Yu, B.M. Kessler, J. Pietzsch, L.A. Kunz-Schughart, The why and how of amino acid analytics in cancer diagnostics and therapy, J. Biotechnol. 242 (2017) 30–54.

[32] L.L. Thomsen, F.G. Lawton, R.G. Knowles, J.E. Beesley, V. Riveros-Moreno, S. Moncada, Nitric Oxide Synthase Activity in Human Gynecological Cancer, Cancer Res. 54 (1994) 1352–1354.

[33] C.S. Cobbs, J.E. Brenman, K.D. Aldape, D.S. Bredt, M.A. Israel, Expression of Nitric Oxide Synthase in Human Central Nervous System Tumors, Cancer Res. 55 (1995) 727–730.

[34] G.L. Semenza, Hypoxia, clonal selection, and the role of HIF-1 in tumor progression, Crit. Rev. Biochem. Mol. Biol. 35 (2000) 71–103.

[35] S. Korde Choudhari, M. Chaudhary, S. Bagde, A.R. Gadbail, V. Joshi, Nitric oxide and cancer: a review, World J. Surg. Oncol. 11 (2013), 118.

[36] J. Muntané, M. De la Mata, Nitric oxide and cancer, World J. Hepatol. 2 (2010) 337–344.

[37] S. Arbault, N. Sojic, D. Bruce, C. Amatore, A. Sarasin, M. Vuillaume, Oxidative stress in cancer prone xeroderma pigmentosum fibroblasts. Real-time and single cell monitoring of superoxide and nitric oxide production with microelectrodes, Carcinogenesis 25 (2004) 509–515.

[38] S. Isik, W. Schuhmann, Detection of nitric oxide release from single cells by using constant-distance-mode scanning electrochemical microscopy, Angew. Chem. Int. Ed. 45 (2006) 7451–7454.

[39] Y. Ha, D. Myung, J.H. Shim, M.H. Kim, Y. Lee, A dual electrochemical microsensor for simultaneous imaging of oxygen and pH over the rat kidney surface, Analyst 138 (2013) 5258–5264.

[40] J.G. Ummadi, C.J. Downs, V.S. Joshi, J.L. Ferracane, D. Koley, Carbon-Based Solid-State Calcium Ion-Selective Microelectrode and Scanning Electrochemical Microscopy: a Quantitative Study of pH-Dependent Release of Calcium Ions from Bioactive Glass, Anal. Chem. 88 (2016) 3218–3226.

[41] Z. Zhu, Q. Zhang, P. Liu, J. Zhang, F. Cao, Quasi-simultaneous electrochemical/chemical imaging of local Fe2+ and pH distributions on 316 L stainless steel surface, J. Electroanal. Chem. 871 (2020), 114107.

[42] Y. Li, K. Hu, Y. Yu, S.A. Rotenberg, C. Amatore, M.V. Mirkin, Direct Electrochemical Measurements of Reactive Oxygen and Nitrogen Species in Nontransformed and Metastatic Human Breast Cells, J. Am. Chem. Soc. 139 (2017) 13055–13062.
[43] K. Hu, Y. Li, S.A. Rotenberg, C. Amatore, M.V. Mirkin, Electrochemical Measurements of Reactive Oxygen and Nitrogen Species inside Single Phagolysosomes of Living Macrophages, J. Am. Chem. Soc. 141 (2019) 4564–4568.
[44] J. Wu, Y. Gao, N. Pan, L. Lu, X. Wang, An isolated single-particle-based SECM tip interface for single-cell NO sensing, Biosens. Bioelectron. 223 (2023), 115048.
[45] A. Kicela, S. Daniele, Platinum black coated microdisk electrodes for the determination of high concentrations of hydrogen peroxide in phosphate buffer solutions, Talanta 68 (2006) 1632–1639.
[46] C.S. Santos, A.S. Lima, D. Battistel, S. Daniele, M. Bertotti, Fabrication and Use of Dual-function Iridium Oxide Coated Gold SECM Tips. An Application to pH Monitoring above a Copper Electrode Surface during Nitrate Reduction, Electroanalysis 28 (2016) 1441–1447.
[47] D.O. Wipf, F. Ge, T.W. Spaine, J.E. Baur, Microscopic measurement of pH with iridium oxide microelectrodes, Anal. Chem. 72 (2000) 4921–4927.
[48] A. Lesch, B. Vaske, F. Meiners, D. Momotenko, F. Cortés-Salazar, H.H. Girault, G. Wittstock, Parallel imaging and template-free patterning of self-assembled monolayers with soft linear microelectrode arrays, Angew. Chem. Int. Ed. 51 (2012) 10413–10416.
[49] S. Daniele, I. Ciani, D. Battistel, Effect of the insulating shield thickness on the steady-state diffusion-limiting current of sphere cap microelectrodes, Anal. Chem. 80 (2008) 253–259.
[50] I. Ciani, S. Daniele, Voltammetric determination of the geometrical parameters of inlaid microdisks with shields of thickness comparable to the electrode radius, Anal. Chem. 76 (2004) 6575–6581.
[51] A. Lesch, P.C. Chen, F. Roelfs, C. Dosche, D. Momotenko, F. Cortés-Salazar, H. H. Girault, G. Wittstock, Finger probe array for topography-tolerant scanning electrochemical microscopy of extended samples, Anal. Chem. 86 (2014) 713–720.
[52] A. Lesch, D. Momotenko, F. Cortés-Salazar, F. Roelfs, H.H. Girault, G. Wittstock, High-throughput scanning electrochemical microscopy brushing of strongly tilted and curved surfaces, Electrochim. Acta 110 (2013) 30–41.
[53] G. Wittstock, M. Burchardt, S.E. Pust, Y. Shen, C. Zhao, Scanning electrochemical microscopy for direct imaging of reaction rates, Angew. Chem. Int. Ed. 46 (2007) 1584–1617.
[54] D. Soltman, V. Subramanian, Inkjet-printed line morphologies and temperature control of the coffee ring effect, Langmuir 24 (2008) 2224–2231.
[55] I.G. Casella, M. Contursi, R. Toniolo, Anodic electrodeposition of iridium oxide particles on glassy carbon surfaces and their electrochemical/SEM/XPS characterization, J. Electroanal. Chem. 736 (2015) 147–152.
[56] J.E. Baur, T.W. Spaine, Electrochemical deposition of iridium(IV) oxide from alkaline solutions of iridium(III) oxide, J. Electroanal. Chem. 443 (1998) 208–216.
[57] B.P. Nadappuram, K. McKelvey, R. Al Botros, A.W. Colburn, P.R. Unwin, Fabrication and characterization of dual function nanoscale pH-scanning ion conductance microscopy (SICM) probes for high resolution pH mapping, Anal. Chem. 85 (2013) 8070–8074.
[58] K. Yamanaka, Anodically electrodeposited iridium oxide films (AEIROF) from alkaline solutions for electrochromic display devices, Jpn. J. Appl. Phys. 28 (1989) 632–637.
[59] H.A. Elsen, C.F. Monson, M. Majda, Effects of electrodeposition conditions and protocol on the properties of iridium oxide pH sensor electrodes, J. Electrochem. Soc. 156 (2009) F1–F6.
[60] B.D. Craig, D.S. Anderson, Handbook of Corrosion Data, 3rd ed., ASM International, 1995.
[61] S. Elzey, V.H. Grassian, Agglomeration, isolation and dissolution of commercially manufactured silver nanoparticles in aqueous environments, J. Nanoparticle Res. 12 (2010) 1945–1958.
[62] S. Goldstein, G. Czapski, Kinetics of Nitric Oxide Autoxidation in Aqueous Solution in the Absence and Presence of Various Reductants. The Nature of the Oxidizing Intermediates, J. Am. Chem. Soc. 117 (1995) 12078–12084.
[63] Y. Wang, J.M. Noël, J. Velmurugan, W. Nogala, M.V. Mirkin, C. Lu, M.G. Collignon, F. Lemaître, C. Amatore, Nanoelectrodes for determination of reactive oxygen and nitrogen species inside murine macrophages, Proc. Natl. Acad. Sci. U.S.A. 109 (2012) 11534–11539.
[64] C. Amatore, S. Arbault, C. Bouton, K. Coffi, J.C. Drapier, H. Ghandour, Y. Tong, Monitoring in real time with a microelectrode the release of reactive oxygen and nitrogen species by a single macrophage stimulated by its membrane mechanical depolarization, ChemBioChem 7 (2006) 653–661.
[65] B.J. Privett, J.H. Shin, M.H. Schoenfisch, Electrochemical nitric oxide sensors for physiological measurements, Chem. Soc. Rev. 39 (2010) 1925–1935.
[66] M. Oliveira, P. Conceição, K. Kant, A. Ainla, L. Diéguez, Electrochemical sensing in 3d cell culture models: new tools for developing better cancer diagnostics and treatments, Cancers (Basel) 13 (2021) 1–21.